Analyst

PAPER

View Article Online
View Journal | View Issue



Cite this: *Analyst*, 2017, **142**, 3747

# Online monitoring of hepatic rat metabolism by coupling a liver biochip and a mass spectrometer†

Franck Merlier,[a] Rachid Jellali *[b] and Eric Leclerc*‡[b]

A microfluidic liver biochip was coupled with a mass spectrometer to detect in real time the drug metabolism of hepatocytes. The hepatocytes were cultivated in the biochip for 35 h. The biochip was placed in a small-scale incubator in which the temperature and $CO_2$ concentration were controlled. The biochip was connected serially to a mass spectrometer, a peristaltic pump and a culture medium reservoir. The injection in the mass spectrometer was performed every 10 min for 11 h. The metabolism of midazolam, phenacetin, omeprazole, dextromethorphan, repaglinide, rosuvastatin, tolbutamide and caffeine was investigated. We monitored the apparition of omeprazole sulfone, hydroxy omeprazole, repaglinide glucuronide, rosuvastatin lactone, dextrorphan, 1-hydroxy midazolam, 4-hydroxy midazolam, 1,4-hydroxy midazolam, paracetamol and 1,3-methylxanthine. Although these were observed, hydroxy-tolbutamide, 3-methoxymorphinan and midazolam glucuronide, hydroxy repaglinide were not detected. Based on a pharmacokinetic model, we calculated *in vitro* intrinsic clearances in which adsorption onto the perfusion circuit was taken into account. Then, using a liver organ model, we extrapolated the *in vitro* intrinsic clearances to the *in vivo* clearances. The estimated *in vivo* clearances were in agreement with the literature data on rats for midazolam, dextromethorphan, phenacetin, tolbutamide and caffeine. Rosuvastatin, omeprazole and repaglinide prediction underestimated the *in vivo* data.

Received 11th June 2017,
Accepted 17th August 2017

DOI: 10.1039/c7an00973a

rsc.li/analyst



## 1. Introduction

The strong contribution of Chemical Reactive Metabolites (CRMs) in Drug Induce Liver Injury (DILI), including idiosyncratic hepatotoxicity, is acknowledged by the scientific community but cannot be detected by conventional animal toxicity studies. Some compounds have progressed into human trials and have then caused severe human toxicity and no patterns existed in the animal studies that signaled these events (interspecies differences in bioavailability, distribution and metabolism may also explain a number of false positives and false negatives). Moreover, in the new fast-track metabolism strategy of industries, there are very few *in vivo* animal metabolism studies to validate the *in vitro–in vivo* correlation (IVIV) of biotransformation for the early prediction of metabolism *in vivo* in humans. It seems clear today that current static *in vitro* test systems (microsomes, hepatocytes, *etc.*) are poorly predictive of human *in vivo* metabolism and toxicity potentially for three reasons: (i) physiological gap between the cells currently used (static mode) and human hepatocytes as they exist in their native state (dynamic mode), (ii) lack of physiological integration with other cells and systems within the liver that are required to amplify the initial toxicological lesion into overt toxicity; (iii) no way to assess how low level cell damage induced by a drug may, under certain circumstances, lead to overt DILI in only a small minority of patients (*i.e.* idiosyncratic hepatotoxins).

Microfluidic bioreactors integrating microstructured topography and dynamic culture conditions have appeared as a potential alternative for mimicking *in vivo*-like liver structures.[1–4] Cells cultivated in such devices can adhere onto the walls of microchannels and microchambers placed in bioreactors. The perfusion of culture medium inside the cell culture area improves the metabolic waste removal and continually renews the nutrient supply. Furthermore, the flow creates "physiological-like" situations such as liver zonation or shear stress on the hepatic tissues.[5,6] Finally, a microenvironment of a few microliters induced by the microchambers enhances cell–cell interactions, reducing the dilution of the chemokines or other chemicals, when compared to the volume of medium involved in plate cultures.[7–9]

[a]*Sorbonne Universités, FRE CNRS 3580, Génie Enzymatique et Cellulaire, Université de Technologie de Compiègne, 60205 Compiègne Cedex, France*
[b]*Sorbonne Universités, CNRS UMR 7338, Laboratoire de Biomécanique et Bio ingénierie, Université de Technologie de Compiègne, Centre de Recherche de Royallieu, BP20529, 60205, France. E-mail: eric.leclerc@utc.fr, rachid.jellali@utc.fr*

†Electronic supplementary information (ESI) available. See DOI: 10.1039/c7an00973a

‡Present address CNRS UMI 2820; Laboratory for Integrated Micro Mechatronic Systems, Institute of Industrial Science, University of Tokyo; 4-6-1 Komaba, Meguro-ku; Tokyo 153-8505, Japan.

With the continuous development of microfabrication and microfluidic technology, microfluidic bioreactors offer many perspectives to cell culture and analysis. Microfluidic systems can be easily automated, allowing the realization of long-term cell cultures under precise conditions without manual intervention. Continuous perfusion of culture medium is generally performed by using micropumps or valves integrated in microfluidic bioreactors.[10–13] In the last few years, several automatic cell cultures in microfluidic devices without micropumps have also been reported in the literature.[14,15] Microfluidic bioreactors offer the advantages of incorporating analytical biosensors into the culture platform.[16] These sensors can provide rapid, non-invasive and non-destructive online analyses, such as temperature, pH, and oxygen, carbon dioxide and glucose concentrations.[16,17] Microbioreactors also allow real time monitoring by coupling with different analytical techniques (chemiluminescence, fluorescence, electrochemistry, mass spectroscopy and chromatography).[16,18–20] Compared to standard cultures in Petri dishes, the use of microfluidic devices provides many possibilities to co-culture cells. Different cell types can be cultivated in separated microbioreactors or compartmented bioreactors, where the cell–cell interactions are ensured by exchange of soluble factors.[10,21,22] In other approaches, cells are cultivated in a single microbioreactor with a pre-treated surface (micropatterning or chemical treatment), allowing the selective adhesion of various types of cells.[10,23] In addition to the advantages cited above, microfluidic bioreactors make it possible the single cell culture and analysis, high parallelization of experiments and high throughput of samples.[10,16,19]

Previously, we showed that hepatocytes cultivated in a microfluidic biochip maintained the activity of their main enzymes for xenobiotic metabolism (various *CYP*, several *SULT* and *UGT* subfamilies and some phase 3 transporters such as *MDR1* and *MRP2*) probably due to a stress response enhanced in the biochips.[24–28] Furthermore, rat hepatocytes cultivated in a biochip coupled with a pharmacokinetic *in silico* model was used to estimate *in vitro* hepatic intrinsic drug clearances. *In vivo* extrapolation based on the *in vitro* biochip data lead to the prediction of *in vivo* hepatic clearances, consistent with the *in vivo* literature data on rats.[29] More generally, it is believed that the use of *in vitro* data in the *in silico* model would be an alternative to reduce animal testing and to predict human pharmacokinetics.[30,31] In parallel, the concept of online monitoring of drug metabolism and its kinetics, using a liver biochip culture and a chromatography method, was illustrated with diclofenac.[20] This direct online analysis can provide accurate kinetics, and specific metabolism behaviour can be ultimately investigated. In this paper, we extended these developments with other drugs. We propose a pharmacokinetic liver biochip strategy by coupling our liver biochip experimental setup to a real time and direct mass spectrometry continuous analysis. Then, the monitored kinetics was simulated using an *in silico* model. Finally, the *in vivo* hepatic clearances were extrapolated and compared with the literature data.

# 2. Materials and methods

## 2.1. Chemical reagents

To analyze the metabolism of the rat hepatocytes, we used phenacetin (PHE) and caffeine (CAF) as *CYP1A* substrates, midazolam (MDZ) as the *CYP3A* substrate, dextromethorphan (DEXTM) as the *CYP3A* and *CYP2D* substrate, tolbutamide (TOLB) as the *CYP2C* substrate, omeprazole (OME) as the *CYP3A* and *CYP2C* substrate, rosuvastatin (ROV) as the *OATP* substrate and repaglinide (REP) for the *CYP2C* substrate. The use of drugs such as CAF and TOLB allowed the analysis of slow metabolism whereas MDZ allowed fast metabolism analysis.

Acetaminophen (APAP), acetaminophen glucuronide (APAP-GLU), caffeine (CAF), paraxanthine (PARA), dextromethorphan (DEXTM), dextrorphan-D-tartrate (DEX), 3-methoxymorphinan hydrochloride (3-MM), midazolam maleate salt (MDZ), 1-OH midazolam (1-OH-MDZ), 4-OH midazolam (4-OH-MDZ), omeprazole (OME), repaglinide (REP), tolbutamide (TOLB) and rosuvastatin (ROV) were purchased from Sigma-Aldrich (St Quentin Fallavier, France). 5-OH omeprazole (5-OH-OME) and 4-OH tolbutamide (4-OH-TOLB) were obtained from SPI-Bio (Montigny Le Bretonneux, France). Omeprazole sulfone (OME-SULF) was obtained from @rtMolecule (Poitiers, France). All solutions were prepared at 10 μM. PHE and MDZ were mixed and analyzed in the same runs. CAF, REP, DEX, OME, TOLB and ROV were mixed and analyzed in parallel. Table 1 summarizes the parent drugs and metabolites studied in this work.

HPLC solvents and atrazine (ATZ) were purchased from Biosolve Chimie (Dieuze, France) and Sigma-Aldrich (St Quentin Fallavier, France), respectively.

## 2.2. Cell culture medium

The seeding medium is composed of William's E Glutamax medium (Fisher Scientific) supplemented with 6.25 μg $ml^{-1}$ of Insulin–Transferrin–Selenium (ITS) (Becton Dickinson, Biosciences), 100 units per mL of penicillin, and 100 mg $mL^{-1}$

**Table 1** Summary of the used drugs and their metabolites

| Parent drug | Metabolite |
|---|---|
| Caffeine (CAF) | Paraxanthine (PARA)<br>1,3-Methylxanthine |
| Dextromethorphan (DEXTM) | Dextrorphan (DEX)<br>3-Methoxymorphinan (3-MM) |
| Midazolam (MDZ) | 1-OH midazolam (1-OH-MDZ)<br>4-OH midazolam (4-OH-MDZ)<br>1,4-OH midazolam (1,4-OH-MDZ) |
| Omeprazole (OME) | 5-OH omeprazole (5-OH-OME)<br>Omeprazole sulfone (OME-SULF) |
| Phenacetin (PHE) | Acetaminophen (APAP) |
| Repaglinide (REP) | UGT repaglinide (UGT-REP) |
| Rosuvastatin (ROV) | Rosuvastatin lactone (ROV-lactone) |
| Tolbutamide (TOLB) | 4-OH tolbutamide (4-OH-TOLB)<br>OH tolbutamide (OH-TOLB) |

of streptomycin (Fisher Scientific) and bovine fetal serum (10%). Culture medium is composed of William's E Glutamax medium supplemented with 6.25 μg $ml^{-1}$ of Insulin-Transferrin-Selenium (ITS) (Becton Dickinson, Biosciences), 100 units per mL of penicillin, and 100 mg $mL^{-1}$ of streptomycin (Fisher Scientific), 5 ng $mL^{-1}$ of dexamethasone (Sigma-Aldrich) and 3 mg $mL^{-1}$ of bovine serum albumin (Sigma-Aldrich).

### 2.3. Rat hepatocyte isolation and cultures

Primary rat hepatocytes were isolated from 5-week-old male Sprague–Dawley rats (Janvier Labs, France) using the two-step method of Seglen.[32] The rats were housed in ventilated, humidity- and temperature-controlled rooms with a 12/12 h light/dark cycle, with food and water *ad libitum*. All procedures were performed with the approval of the Veterinary Authorities of France in accordance with the European Communities Council Directive of 22nd September 2010:63/UE. This study was specifically approved by the Université de Technologie de Compiègne ethics committee. After animal anesthesia by injection of sodium pentobarbital, the liver was perfused with buffer solution (HEPES/EGTA) and digested using collagenase. Then, the liver was extracted, deposited in Dulbecco's Modified Eagle's Medium (DMEM, Gibco – Life Technologies) and the tissue was gently disrupted. The digested tissues were filtered through 100 μm filters and the liver cell suspensions were centrifuged (50 g, 5 min, three times). The resulting pellets were mixed, suspended in an Easycoll separating solution (Biochrom AG – Merck Millipore) prepared in DMEM medium with a final density of 36%, and centrifuged (168 g, 20 min). Percoll isogradient centrifugation was performed to isolate dead cells and a significant portion of the nonparenchymal cells in a floating top layer was discarded. Finally, the obtained cells were suspended in seeding medium. Cell viability was assessed by Trypan blue dye exclusion and hepatocyte culture with a viability of more than 90% was used.

Primary rat hepatocytes were cultivated in microfluidic biochips made of polydimethylsiloxane (PDMS). The design and dimensions of the biochip have been described in our previous work.[33,34] Biochips were sterilized using an autoclave, coated with collagen (BD Biosciences) at 300 μg $mL^{-1}$ and incubated at 37 °C and 5% $CO_2$. After 1 h, the collagen solution was washed using the seeding medium and the freshly isolated hepatocytes ($5 \times 10^5$ cells per biochip) were loaded into the microfluidic device *via* biochip inlet ports using a micropipette tip. To keep the seeding medium inside the culture chamber, the biochip inlet ports were closed using two syringes (containing 500 μL of seeding medium), and the biochips were placed in an incubator at 37 °C and 5% $CO_2$. After 24 h of static conditions to promote cell adhesion, the seeding medium was replaced by the culture medium and the biochip was integrated in the experimental setup.

At the end of the experiment (11 h of dynamic culture and online analysis), the biochip was detached from the experimental setup and double staining using calcein AM and propidium iodide (PI) was carried out to perform *in situ* visualizations of live and dead cells. Briefly, a solution of culture medium containing propidium iodide (50 nM) and calcein AM (2 μM) was added and the biochip was incubated at 37 °C, 5% $CO_2$. After 20 min, the biochip was rinsed and observed using a conventional fluorescence microscope (Leica DMI 6000B).

### 2.4. Experimental setup: biochip/mass spectrometer coupling

After the cell adhesion step and culture medium change, the biochips were integrated in a small-scale incubator and serially connected to the experimental setup (Fig. 1A and B). In addition to the small-scale incubator, the main equipment of the experimental setup consists of a peristaltic pump, two controllers for temperature and $CO_2$ concentration, a culture medium reservoir, two 6-way valves, an HPLC system and a mass spectrometer. The small-scale incubator was connected to the controllers (Pecon Gmbh) allowing the control of the temperature and the $CO_2$ concentration around the biochip. The flow rate was controlled by using a peristaltic pump and set at 25 μL $min^{-1}$. The drugs were added into the culture medium in the reservoir at 10 μM. The culture medium (2 μL) was injected every 10 min in the mass spectrometer. The analysis was performed in positive and negative modes alternatively, leading to a measure in each mode every 20 min. Once the mass spectrometry analysis was performed, before the injection of the next sample, the injection loop was washed using water and dried by air perfusion.

The biochip was connected to the mass spectrometer by a system of two 6-way valves (Fig. 1B and Fig. S1†). Every 10 minutes, the valve system undergoes a three-step cycle (Fig. S1†): (1) collection of culture medium *via* the sampling loop, (2) injection of the collected culture medium and the internal standard by using an automatic injector, and start of

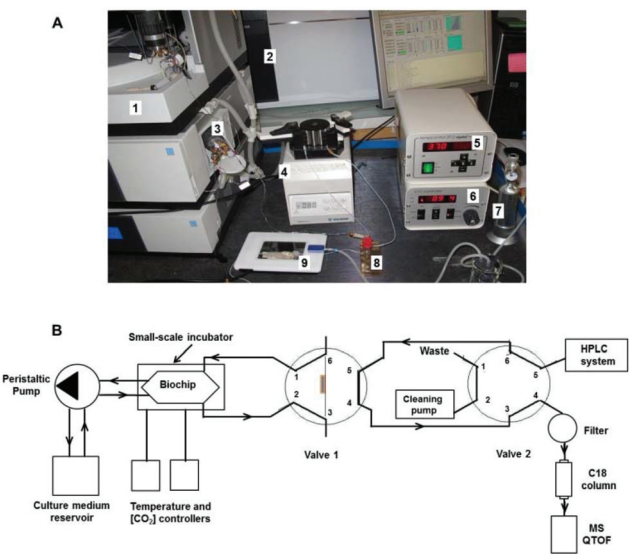


Fig. 1 Picture (A) and schematic overview (B) of the experimental set-up allowing microfluidic biochip culture and online injection in a mass spectrometer: (1) HPLC system; (2) mass spectrometer; (3) valve; (4) peristaltic pump; (5) temperature controller; (6) $CO_2$ controller; (7) $CO_2$ tank; (8) culture medium reservoir and (9) small-scale incubator.

the chromatographic separation/detection by LC-HR/MS in positive or negative mode, (3) washing of the injection loop. During steps 2 and 3, the biochip is isolated from the LC-HR/MS system. At the end of the cycle, the HPLC system is reset and the collection cycle is restarted.

### 2.5 Mass spectrometry analysis

A Dionex HPLC system was used for liquid chromatography. The system consists of a dual gradient pump (DGP 3000 RS) with an integrated degasser (U3000 RSLC with a SRD 6 channel), an auto-injector (WPS-3000RS), a column thermostat (TCC-3000RS) with an external 6-way valve, a FlowManager (FLM-3000) with an integrated external 10 position valve, and a UV/VIS detector (DAD-3000RS). The HPLC system was controlled by using Chromeleon 6.8 software.

LC-HRMS was performed using an Agilent 6538 UHR QTOF mass spectrometer with an electrospray ion source. LC separation was performed on a Zorbax extend C18 (Agilent) (100 A, 50 × 2.1 mm, 1.8 μm) column connected to a DIONEX pump. Atrazine was used as an internal standard. Mobile phase A consisted of 100% HPLC grade water with 0.1% formic acid and mobile phase B consisted of 100% HPLC grade acetonitrile. The gradient program began with 0% B, ramped to 95% B at 5 min, held at 95% for 1 min, returned to the initial conditions and remained constant for 2.25 min. The flow rate was 0.5 mL $min^{-1}$. The mass spectrometer was operated alternatively in positive and negative ESI modes. Nitrogen was used as a nebulizer. The capillary voltage was +3500 V and −3500 V, respectively, and the ion source gas temperature was 350 °C, with a flow rate of 12 L $min^{-1}$. The fragmentor was set at 130 V and the nebulizer at 30 psi. The mass range was set from 100 to 1500 *m/z*. Full scan mode and all ion fragmentation modes at 20 eV were used at a 2 Hz frequency. The mass detection was performed using the exact mass of pseudo-molecular ions ($[M + H]^+$, $[M + Na]^+$ or $[M - H]^-$) with a confidence interval of 20 ppm for the automatic search mode, and less than 5 ppm for manual identification. For the manual identification, the mass was calculated from the molecular formula (Table S1†) and confirmed by the retention time and the MS/MS experiment.

### 2.6. The kinetic model for drugs *in vitro*

The model is similar to our previous work describing rat primary hepatocyte clearance in biochips.[35] The drug kinetics in the perfusion systems was described using a three-compartment model. This model includes one reservoir, the hepatic biochip and a compartment representing the tubing between the biochip and the reservoir. Even though serum was not used in the experiments, we modelled a binding of the drugs to the proteins of the culture medium *via* the parameter $fu_{med}$. The hepatocytes effectively produced albumin in the biochip cultures which may contribute to binding of the compounds (few hundreds ng per h per $10^6$ cells, data not shown). Non-specific binding to the perfusion system was set *via* previously dedicated adsorption experiments and then modelled to occur in the tube. A first-order relationship rate was assumed for metabolism because we expected linear metabolism at the low doses used in our experiments. The perfusion was recirculating in the biochips but the volume sampling was not taken into account. These assumptions led to the derivation of a set of first-order differential equations:

$$\frac{dQ_{R1}(t)}{dt} = F \times (C_T(t) - C_{R1}(t)) \quad (1)$$

$$\frac{dQ_{HepB}(t)}{dt} = F \times (C_{R1}(t) - C_{HepB}(t)) - fu_{med} CL_{int,invitro} C_{HepB}(t) \quad (2)$$

$$\frac{dQ_T(t)}{dt} = F \times (C_{HepB}(t) - C_T(t)) - \frac{dQ_{Ads}(t)}{dt} \quad (3)$$

where, the subscripts R1, HepB, and T correspond to the reservoir, the hepatic biochip and tubing compartments, respectively, $F$ is the flow rate in the recirculating perfusion system (25 μL $min^{-1}$), $C_i$ is the concentration in the compartment $i$, $Q_i$ is the amount in the compartment $i$, $C_i$ and $Q_i$ are related to the volume $V_i$ as follows: $C_i = Q_i/V_i$ with $V_{R1}$ = 2 mL, $V_{HepB}$ = 40 μL, $V_T$ = 0.5 mL, $CL_{int,in\ vitro,}$ is the *in vitro* intrinsic clearance (to be estimated by the model), $fu_{med}$ is the unbound drug fraction in the culture medium, $Q_{ads}$ is the quantity adsorbed in the tubing circuit. The latter is given by the following equation:

$$\frac{dQ_{Ads}(t)}{dt} = k_b \times C_T(t) - k_u Q_{Ads}(t) \quad (4)$$

where, $k_b$ is the adsorption rate for non-specific binding on the walls (tubes, reservoirs, and biochips) and $k_u$ is a dissociation constant. We used the values estimated in our previous experiments and models (Table 2).

The kinetics of the metabolite(s) was described with a similar model. For one metabolite (subscript Met), the model is:

$$\frac{dQ_{R1,Met}(t)}{dt} = F \times (C_{T,Met}(t) - C_{R1,Met}(t)) \quad (5)$$

$$\frac{dQ_{HepB,Met}(t)}{dt} = F \times (C_{R1,Met}(t) - C_{HepB,Met}(t)) + fu_{med,met} CL_{int,invitro,met} \times C_{HepB}(t) \quad (6)$$

$$\frac{dQ_{T,Met}(t)}{dt} = F \times (C_{HepB,Met}(t) - C_{T,Met}(t)) - \frac{dQ_{Ads,Met}(t)}{dt} \quad (7)$$

$$\frac{dQ_{Ads,Met}(t)}{dt} = k_{bMet} \times C_{T,Met}(t) - k_{uMet} Q_{AdsMet}(t) \quad (8)$$

The metabolite formation and parent drug clearance were linked by the terms $CL_x C_{HepB}$ in eqn (2) and (6). We calculated and solved the equations using the concentrations in mol to respect the stoichiometry. The set of equations was solved using the "R" software and the "deSolve" package. The clearances $CL_x$ were estimated and optimized using the experimental results (Table 2).

 

Table 2 Estimated parameters for the kinetic model and comparison with the literature data

| | | | | $CL_{int,\ in\ vitro}$ (μL per min per $10^6$cells) | |
|---|---|---|---|---|---|
| | $fu_{med}$ | $k_b$ (μL $min^{-1}$) | $k_u/k_b$ (μ$L^{-1}$) | Estimated from the model | Literature data |
| CAF | 0.99[a 45] | 0.05[c] | 0[c] | 6 | 1.4[37] 0.58[42] |
| 1,3-Methylxanthine | 0.99[b] | 0[b] | 0[b] | 6 | — |
| OME | 0.8[41] | 0.161[c] | $0.17 \times 10^{-3}$ [c] | 18 | 7.4[41] |
| OME-SULF | 1[b] | 0[b] | 0[b] | 12 | — |
| OME-SULF-X | 1[b] | 0[b] | 0[b] | 5.4 | — |
| OH-OME | 1[b] | 0[b] | 0[b] | 6 | — |
| OH-OME-X | 1[b] | 0[b] | 0[b] | 180 | — |
| DEXTM | 0.85[40] | 0.033[c] | $0.009 \times 10^{-3}$ [c] | 180 | 110[37] 105[38] 76[40] |
| DEX | — | — | — | ND | 54[38] 28.4[40] 545[47] |
| MDZ | *0.54*[a 48] | 1.1[c] | $0.15 \times 10^{-3}$ [c] | 120 | 74[37] 110[43] |
| 1-OH-MDZ | 1 | 0[b] | 0[b] | 24 | 16 ± 7[47] |
| 1-OH-MDZ-X | 1 | 0[b] | 0[b] | 30 | — |
| 4-OH-MDZ | 1 | 0[b] | 0[b] | 18 | 12 ± 7[47] |
| 4-OH-MDZ-X | 1 | 0 | 0[b] | 36 | — |
| 1,4-OH-MDZ | 1 | 0[b] | 0[b] | 66 | — |
| 1,4-OH-MDZ-X | 1 | 0[b] | 0[b] | 600 | — |
| PHE | 0.977[a 46] | 0.2[c] | $1.2 \times 10^{-3}$ [c] | 36 | 78[37] |
| APAP | 0.93[39] | 0[c] | 0[c] | 36 | 14.8[39] |
| REP | 0.94[44] | 0[b] | 0[b] | 6 | 60–120[44] |
| UGT-REP | 1[b] | 0[b] | 0[b] | 6 | 0.33–1.4[44] |
| TOLB | 0.99[a 45] | 0[c] | 0[c] | 2.4 | 1.6[37] |
| OH-TOLB | — | — | — | ND | 1.14[47] |
| ROV | 0.83[44] | 0[b] | 0[b] | 6 | 9–36[49] |

[a] Denotes data from human sources. [b] Parameter set as parent drugs or to 1 and 0, due to the lack of literature information, ND not evaluated/detected compounds. [c] Home data and fitted with adsorption experiments from Prot *et al.*,[25] Baudoin *et al.*,[35] Baudoin *et al.*,[29] and Habka[36].

### 2.7. Prediction of *in vivo* rat intrinsic hepatic clearances

The *in vitro* intrinsic clearances expressed per cell estimated from the *in vitro* experiments were scaled to correspond to the *in vivo* intrinsic clearance. For this purpose, a scaling factor was applied to express the *in vitro* intrinsic clearances in ml per min per kg of body mass. The hepatocellularity was set to $109 \times 10^6$ hepatocytes per gram of liver,[50] and the liver weight to 40 grams per kilogram of body mass in the case of rats. The multiplication of these two quantities defines the scaling factor (SF) equal to $4360 \times 10^6$ hepatocytes per kilogram of body mass for *in vitro*/*in vivo* extrapolation of the intrinsic clearance.

$$CL_{int,in\ vivo} CL_{int,in\ vitro} \times SF \quad (9)$$

Extrapolation of the hepatic intrinsic clearance to the *in vivo* clearance is usually performed *via* models with a different degree of complexity that describes blood dispersion within the liver.[51–53] The three typical models (well-stirred, parallel tube and dispersion models) have been shown to exhibit minor differences for a wide range of drugs.[37] For this reason, the well-stirred model was used primarily in this study. The hepatic clearance is then given as:

$$CLh = \frac{Q_H \times \frac{fu_b}{fu_{med}} \times CL_{int,invitro} \times SF}{Q_H + \frac{fu_b}{fu_{med}} \times CL_{int,invitro} \times SF} \quad (10)$$

where the liver blood flow, $Q_H$, was set to 86 ml per min per kg of rat bodyweight[37,54,55] and the unbound fraction of the drug in blood ($fu_b$) was set according to the literature data (Table 3). The intrinsic clearances estimated under these experimental conditions were then used to derive the hepatic clearance.

## 3. Results

### 3.1 Experimental analysis

**3.1.1 Cell culture during the online integration.** The rat hepatocytes were successfully attached inside the cell culture chamber of the biochips. The entire surface of the biochips was covered by the cells. Hepatocytes displayed typical cuboid shapes (Fig. 2A) after 24 h of rest. After the 48 h perfusion either in control experiments in a conventional incubator (Fig. 2B) or in a portable incubator, without online coupling, we did not detect any morphological difference. We also did not detect any effect on the cell morphology after the integration with the mass spectrometer without drug assays (Fig. 2C). The hepatocyte confluence was still observed in the biochip. This preliminary analysis demonstrated the potential of the portable incubator.

However, we found that the integration was only stable for a few hours when the culture medium samples were injected

Table 3 Prediction of the *in vivo* intrinsic and hepatic clearances using a well-stirred model

| | Selected data from the literature to run the models | | Biochip model predictions (ml per min per kg of BDW) | | Literature data (ml per min per kg of BDW) |
|---|---|---|---|---|---|
| | $fu_{med}$ | $fu_b$ | $CL_{int,\ in\ vivo}$ | $CLh_{in\ vivo}$ | $CLh_{in\ vivo}$ |
| CAF | 0.99[45a] | 1[37] | 26 | 20 | 12[37]–13[42] |
| 1,3-Methylxanthine | 0.99[b] | 0.85[57c] | | | |
| DEXTM | 0.85[40] | 0.45[38] | 785 | 71 | 80[37] |
| MDZ | 0.54[48a] | 0.07[37] | 523 | 40 | 44[37]–74.3[59]–130[43] |
| 1-OH-MDZ | 1[b] | 0.04[59] | 105 | 4 | 62.2[59] |
| 4-OH-MDZ | 1[b] | 0.04[b] | 78 | 3 | — |
| 1,4-OH-MDZ | 1[b] | 0.04[b] | 288 | 10 | — |
| OME | 0.8[41] | 0.16[39] | 75 | 13 | 52[59]–710[39] |
| OME-SULF | 1[b] | 0.02[58] | 52 | 1 | — |
| 5-OH-OME | 1[b] | 0.17[58] | 26 | 4 | — |
| PHE | 0.977[46a] | 1[37] | 157 | 56 | 84[37] |
| APAP | 0.93[39] | 0.82[39] | 26 | 18 | 23.8[39] |
| ROV | 0.094[56a] | 0.83[44] | 26 | 2.9 | 50[49] |
| REP | 0.0074[56a] | 0.94[44] | 26 | 0.2 | 27[60] |
| TOLB | *0.99*[45a] | *0.08*[37] | *10.5* | *0.84* | *1.6*[38]–*0.48*[37] |

[a] Denotes data from human sources. [b] Parameter set as parent drugs or metabolites or to 1 due to the lack of literature information. [c] Set as para-xanthine due to the lack of data.

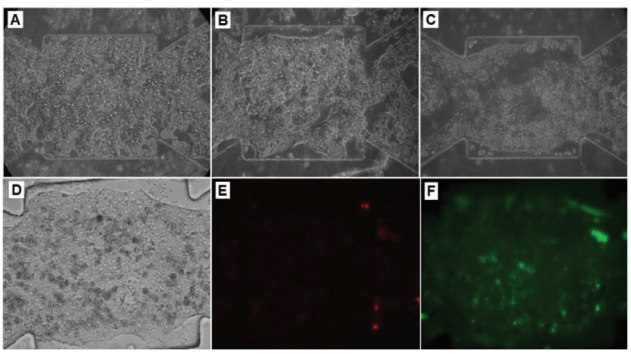


Fig. 2 Hepatocyte morphology (A) before perfusion; (B) after 48 h of perfusion in the conventional $CO_2$ incubator; (C) after 48 h of perfusion including 24 h within the portable incubator and with the mass spectrometer circuit; (D) after 11 h of drug kinetics and online analysis with the mass spectrometer; (E) and (F) propidium iodide and calcein AM stainings at the end of the drug kinetics experiments.

into the spectrometer. This was due to the blocking of the filter located at the inlet of the injection loop. When blocked, the injection sequence created an over pressure in the perfusion loop leading to the breakage of the circuit at the mass spectrometer inlet. As a result, the continuous injection and analysis, with a frequency of every 10 min, was possible for only 11 h. Thus the experimental analysis results of the 24 h adhesion step followed by 11 h of perfusion (leading to 35 h of culture) were obtained.

When the drug assays were performed, we did not detect any morphological change. The cells were healthy as demonstrated by the calcein AM staining. Only a few necrotic cells were positive to IP for all tested conditions (Fig. 2D–F).

**3.1.2 Parent drug kinetics.** The drugs were loaded in the culture medium tank. We observed an increase in the quantity of the drug in the mass spectrometry injected sample in the first hour of perfusion. This corresponded to the time of homogeneous mixing of drug in the overall culture medium loop (2.5 mL culture medium flowed at 25 μL $min^{-1}$ need 100 min for one turn).

Once we reached a peak, we monitored an important and continuous decrease of MDZ, PHE, OME and DEXTM (Fig. 3A, E, 4A and 6A, respectively). Concerning CAF, REP, ROV and TOLB (Fig. 5A, C, E and 6B, respectively), the decrease of the level of those drugs was very slow but were clearly observed over the 11 h of monitoring. The chromatograms of all drugs are shown in Fig. S2.†

**3.1.3 Metabolite kinetics.** The presence of the metabolites was detected for 20 min for MDZ, OME, DEXTM, REP, ROV, CAF and PHE. Fig. S3 and S4† show the typical chromatograms of MDZ and OME and their metabolites after 200 min. Although we searched in the samples, we never found OH-TOB and 3-MM. We measured a continuous increase of the levels of 1,4-OH-MDZ (Fig. 3B) for the first 130 min, 1-OH-MDZ and 4-OH-MDZ (Fig. 3C and D), and 5-OH-OME and OME-SULF (Fig. 4B and C) for the first 200 min and 1,3-methylxanthine, UGT-REP and ROV-lactone (Fig. 5B, D and F) for the first 280 min. Then the levels of these molecules tend to stabilise (such as 1-OH-MDZ, 4-OH-MDZ, OME and OME) or decline continuously (ROV-lactone). The APAP production followed a global tendency to increase in the culture medium (Fig. 3F). Although DEX and PARA were detected, the tendencies of the kinetics were not clear (Fig. S5†) due to the too high noise ratio.

### 3.2 Pharmacokinetic modelling

**3.2.1 Hepatic intrinsic *in vitro* clearances.** The experimental values were used to estimate the *in vitro* hepatic intrinsic clearances. To calculate the clearance, we took into account the parent drug adsorption on the wall and pipes of the perfusion loop using our previous data (we calibrated this phenomenon for these drugs in our previous studies). Thus,

 

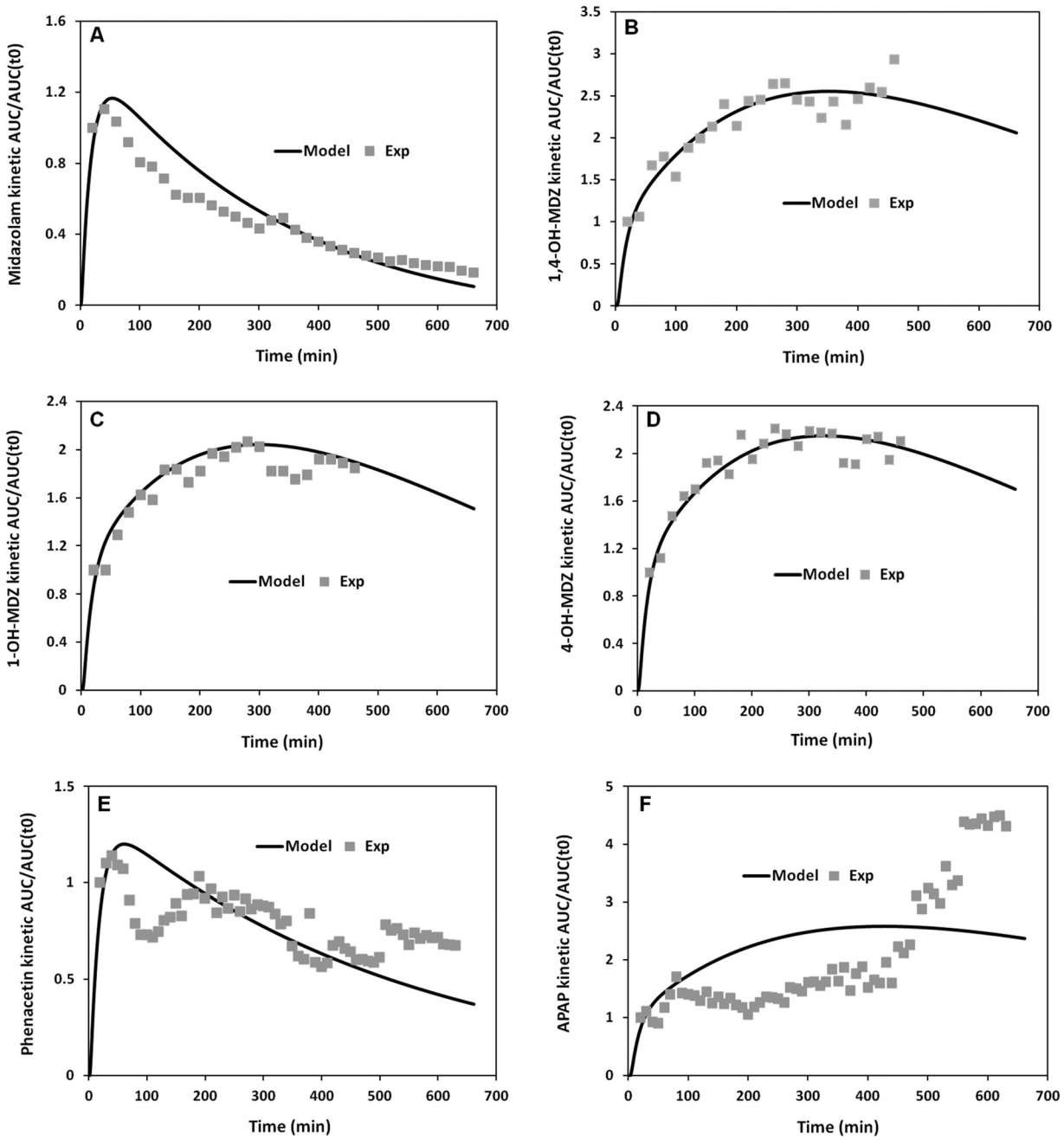


**Fig. 3** Comparison of the experimental and modelled kinetics of midazolam (A); 1,4-OH-MDZ (B); 1-OH-MDZ (C); 4-OH-MDZ (D); phenacetin (E) and APAP(F).

the kinetics of the parent drug was reproduced successfully for all compounds. In addition, we were also able to fit the metabolite kinetics of most of the detected compounds such as 1,4-OH-MDZ, 1-OH-MDZ, 4-OH-MDZ, 5-OH-OME and OME-SULF (Fig. 3B–D and 4B, C). However, we were not able to model precisely the metabolite production of APAP (Fig. 3F), ROV-Lactone (Fig. 5F), DEX (not shown) and PARA (not shown).

Then, based on these simulations, we calculated the clearance for all parent drugs and for the detected metabolites as shown in Table 2.

**3.2.2** ***In vivo*** **extrapolation.** Finally, using the well-stirred model, we extrapolated the *in vivo* intrinsic clearances and the hepatic clearances for the parent drugs and their metabolites as shown in Table 3.

## 4. Discussion

In this paper, we present the result of the integration of a liver microfluidic biochip directly connected to a mass spectro-

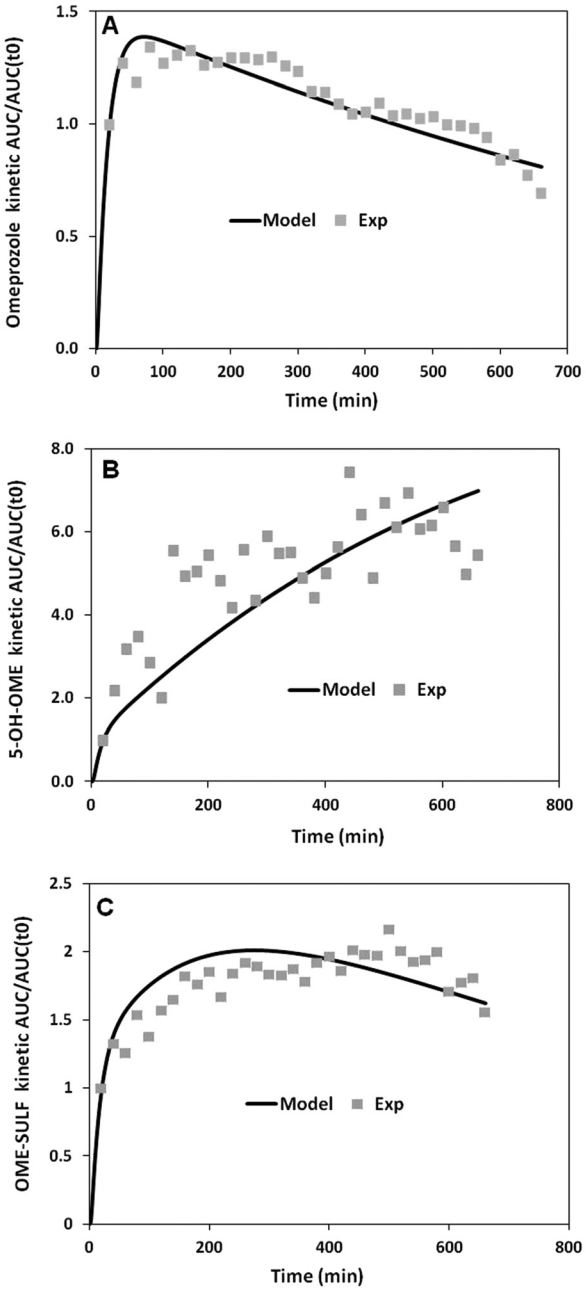


Fig. 4 Comparison of the experimental and modelled kinetics of omeprazole (A); 5-OH-OME (B) and OME-SULF (C).

meter. Thanks to the direct coupling, we were able to monitor continuously the drug metabolism.

The integration was flexible and we were able to determine successfully the kinetics of several drugs over 11 h of culture. At the end of the experiments, the cultures in the control perfusion in the conventional incubator and the culture in the portable set-up display similar viabilities and cell morphologies. The portable cultures were, without injection in the mass spectrometer, maintained for 72 h (24 h of cell adhesion and 48 h of perfusion). However, the online monitoring was successful only for a few hours. The critical point to extend the monitoring up to 48 h of perfusion was the injection loop. A filter should be placed at the entrance to prevent cell dust or big molecules (such as protein) from entering into the spectrometer. This filter induced a limitation for long term kinetics because of protein accumulation. After 12 h of continuous sampling, the filter was systematically blocked leading to an over pressure in the perfusion loop. The pressure contributed to the opening of the perfusion loop. Although the filter can be changed, it creates a discontinuity in the kinetics due to the circuit manipulation and fluid loss (data not shown). In order to facilitate its replacement, the filter was placed between the loop and the chromatography column. Furthermore, it is possible to integrate a bypass system between two filters using an additional valve. Thus, the filter can be replaced without interruption of the kinetics. Finally, we used atrazine as an internal standard. This allowed us to follow, during the course of 11 hours of injections, *i.e.* 66 injections, the possible reduction of the response of the mass spectrometer and, if necessary, to normalize the area of the peaks taking into account this fouling, and the matrix effect.

All tested drugs were successfully detected and their biotransformation was confirmed by the detection of several metabolites. The kinetics of degradation of OME, MDZ and DEXTM (*CYP3A* substrates) was faster when compared to the other studied drugs. In parallel, we found a high continuous production of midazolam and omeprazole metabolites. These results illustrate high *CYP3A* activity in our biochips. Previously, Baudoin *et al.*[29] and Legendre *et al.*[4] evidenced that the *CYP3A* gene is the most upregulated gene in rat hepatocyte cultures in biochips (*CYP3A* level was increased of 20-fold, when compared with the post-extraction values). PHE (*CYP1A* substrate) and especially CAF (*CYP1A*), TOLB (*CYP2C*), ROV (*OATP*), and REP (*CYP2C*) exhibit slow degradation kinetics. However, their biotransformation and the detection of their metabolites demonstrate the functionalities of *CYP1A*, *CYP2C* and *OATP* in our cultures. This result agrees with Baudoin *et al.*,[29,35] who reported an upregulation of these enzymes in rat and human hepatocyte cultures.

The pharmacokinetic model allowed the extraction of the intrinsic *in vitro* clearances. When compared to the literature using microsomes or plated rat hepatocytes,[37,42,44,48,49] we found higher *in vitro* intrinsic clearances for MDZ, DEXTM, CAF, OME and TOLB. In contrast, we found lower *in vitro* intrinsic clearances for PHE, REP and ROV. The extrapolations of the *in vivo* hepatic clearances were similar to the *in vivo* data for DEXTM, MDZ and TOLB. We slightly overestimated the CAF one whereas we slightly underestimated PHE and APAP ones. These results reflect the functional CYP450 enzymes of the hepatocytes in our biochip culture. These results are also consistent with what we measured and estimated in our previous work using a similar microfluidic platform allowing 12 biochip cultures in parallel (with sampling and post-treatment with mass spectrometry measurements after the cell experiment[29]).

By following the drug kinetics, we were also able to propose the kinetics of apparition and the clearance of various

 

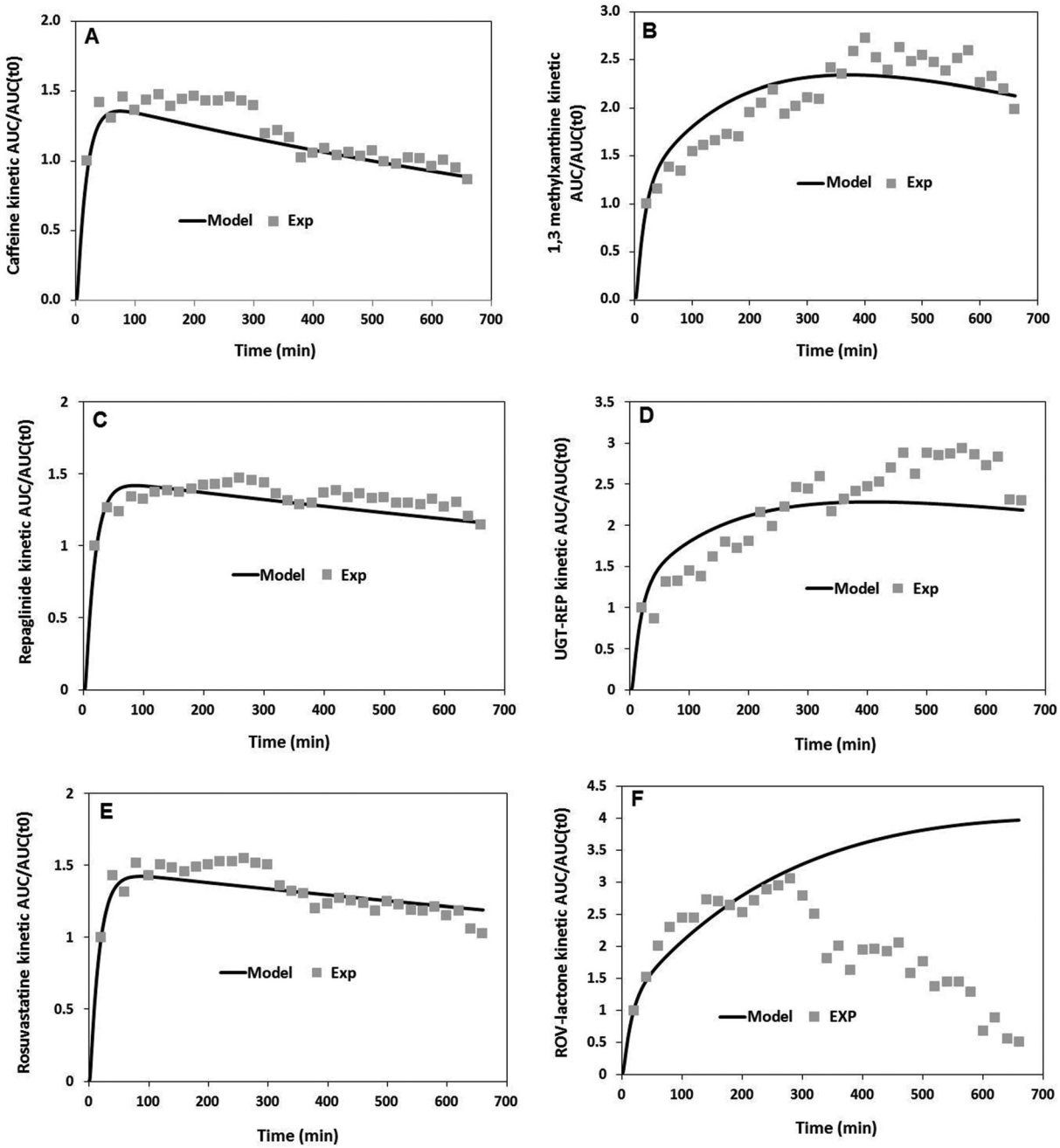


**Fig. 5** Comparison of the experimental and modelled kinetics of caffeine (A); 1,3-methylxanthine (B); repaglinide (C); UGT-REP (D); rosuvastatin (E) and ROC-lactone (F).

metabolites. The estimation of the metabolite clearance did not take into account the adsorption phenomena. Although the metabolites are usually polar and hydrophilic compounds (thus weakly adsorbed on our pipes), our previous studies have shown that about 20%–25% of 1-OH-MDZ, 4-OH-MDZ, and DEX were adsorbed after 4 h of perfusion in our perfusion circuit.[25] In addition, we do not have precise information on the unbound fraction in plasma/blood and the medium binding property. As a result, we underestimated the *in vitro* intrinsic clearances of these compounds. This also leads to the underestimation of the hepatic clearance. More precise calculations of these parameters or additional adsorption experiments will be required to refine our predictions.

Estimated clearances with omeprazole metabolites should be more accurate because no adsorption of OME-S and 5-OH-OME was detected in our previous tests.[25] However, the prediction of the parent drug metabolism was not properly estimated when compared to the literature. Although the intrinsic *in vitro* hepatic clearance was higher than that in one of the literature studies with hepatocytes and microsomes,[41]

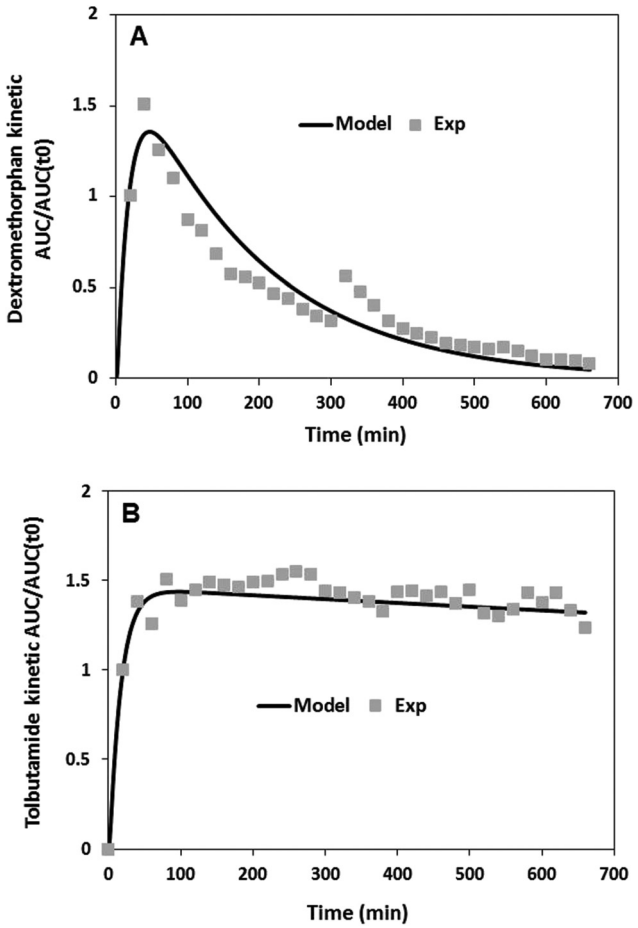


Fig. 6 Comparison of the experimental and modelled kinetics of omeprazole (A); 5-OH-OME (B) and OME-SULF (C).

we predicted an *in vivo* hepatic clearance equal to 13 ml per min per kg of BDW. This value was about 4-fold lower than that in a recently reported *in vivo* study.[59] Although we have no clear explanation for this failure, we can propose several hypotheses. Rat clearances reported in literature correspond to the total clearance which includes the first pass intestine metabolism. In addition, omeprazole follows non-linear metabolism. As a result, a more complex *in vitro* culture and *in silico* model, such as a PBPK model, would be required for more precise *in vivo* extrapolation.

Concerning repaglinide and rosuvastatin, the model predictions were also not accurate. This can be easily understood by the mechanism of the biotransformation of these compounds. Both drugs are partially cleared *via* the bile duct network. This mechanism is not specifically reproduced in our biochip because we did not functionalise yet the liver-on-chip approach up to a bile functional network. In addition, bile metabolism was not modelled in our pharmacokinetic equations. However, these drugs show that we can follow their transport into the hepatocytes (because they are OATP substrates[49,56]). Nevertheless, the presence of REP-glucuronide and ROV-lactone contributed to the illustration of the OATP activity and then the subsequent phase-I and phase-II biotransformation.

# 5. Conclusion

In this paper, we present the results of the integration of a microfluidic culture with a mass spectrometer. The methods allow the continuous monitoring of drug metabolism in a microfluidic biochip. The experimental data, when used with an *in silico* model, allow the estimation of the *in vitro* hepatic intrinsic clearances and the *in vivo* hepatic clearance extrapolation. The method was accurate to predict the clearance of PHE, MDZ, DXM, CAF, and TOLB whereas the prediction remained poor for the REP, ROV and OME. Finally, we continuously follow the kinetics of several metabolites and propose an estimation of their hepatic clearance.

## Conflicts of interest

There are no conflicts to declare.

## Acknowledgements

The analytical equipment (HPLC and MS) used in this work was co-funded by the Regional Council of Picardie and the European Union (CPER 2007–2020). Rachid Jellali was funded by the French Agency for Food, Environmental and Occupational Health & Safety (ANSES, project IMITOMICS-N° EST-2014/1/093).

## References

1 A. Sivaraman, J. K. Leach, S. Townsend, T. Iida, B. J. Hogan, D. B. Stolz, R. Fry, L. D. Samson, S. R. Tannenbaum and L. G. Griffith, *Curr. Drug Metab.*, 2005, **6**, 569–592.
2 P. T. Maguire, E. Novik, K. C. Cheng and M. L. Yarmush, *Biochem. Pharmacol.*, 2009, **78**, 625–632.
3 E. Novik, T. J. Maguire, P. Chao, K. C. Cheng and M. L. Yarmush, *Biochem. Pharmacol.*, 2010, **79**, 1036–1044.
4 A. Legendre, R. Baudoin, G. Alberto, P. Paullier, M. Naudot, T. Bricks, J. Brocheton, S. Jacques, J. Cotton and E. Leclerc, *J. Pharm. Sci.*, 2013, **102**, 3264–3276.
5 J. W. Allen, S. R. Khetani and S. N. Bhatia, *Toxicol. Sci.*, 2005, **84**, 110–119.
6 A. W. Tilles, H. Baskaran, P. Roy, M. L. Yarmush and M. Toner, *Biotechnol. Bioeng.*, 2001, **73**, 379–389.
7 J. Warrick, W. Murphy, J. David and D. Beebe, *IEEE Rev. Biomed. Eng.*, 2008, **1**, 75–93.
8 K. Bhadriraju and C. S. Chen, *Drug Discovery Today*, 2002, **7**, 612–620.
9 E. Knight and S. Przyborski, *J. Anat.*, 2015, **227**, 746–756.
10 D. Gao, H. Liu, Y. Jiang and J. M. Lin, *Trends Anal. Chem.*, 2012, **35**, 150–165.
11 H. Kimura, T. Yamamoto, H. Sakai, Y. Sakai and T. Fujii, *Lab Chip*, 2008, **8**, 741–746.

 

12 L. Liu, K. Loutherback, D. Liao, D. Yeater, G. Lambert, A. Estevez-Torres, J. C. Sturm, R. H. Getzenberg and R. H. Austin, *Lab Chip*, 2010, **10**, 1807–1813.
13 B. J. Toley, J. A. Wang, M. Gupta, J. R. Buser, L. K. Lafleur, B. R. Lutz, E. Fu and P. Yager, *Lab Chip*, 2015, **15**, 1432–1444.
14 P. Novo, F. Volpetti, V. Chua and J. P. Conde, *Lab Chip*, 2013, **13**, 641–645.
15 T. Kim and Y. H. Cho, *Lab Chip*, 2011, **11**, 1825–1830.
16 S. Halldorsson, E. Lucumi, R. Gómez-Sjöberg and R. M. T. Fleming, *Biosens. Bioelectron.*, 2015, **63**, 218–231.
17 P. Gruber, M. P. C. Marques, N. Szita and T. Mayr, *Lab Chip*, 2017, **17**, 2693–2712.
18 Q. Chen, J. Wu, Y. Zhang and J. M. Lin, *Anal. Chem.*, 2012, **84**, 1695–1701.
19 C. Rivet, H. Lee, A. Hirsch, S. Hamilton and H. Lu, *Chem. Eng. Sci.*, 2011, **66**, 1490–1507.
20 P. M. van Midwoud, J. Janssen, M. T. Merema, I. A. de Graaf, G. M. Groothuis and E. Verpoorte, *Anal. Chem.*, 2011, **83**, 84–91.
21 M. Tehranirokh, A. Z. Kouzani, P. S. Francis and J. R. Kanwar, *Biomicrofluidics*, 2013, **7**, 051502.
22 L. Choucha-Snouber, C. Aninat, L. Grsicom, G. Madalinski, C. Brochot, P. E. Poleni, F. Razan, C. Guguen Guillouzo, C. Legallais, A. Corlu and E. Leclerc, *Biotechnol. Bioeng.*, 2013, **110**, 597–608.
23 E. Leclerc, K. El Kirat and L. Griscom, *Biomed. Microdevices*, 2008, **10**, 169–177.
24 J. M. Prot, C. Aninat, L. Griscom, F. Razan, C. Brochot, C. Guguen Guillouzo, C. Legallais, A. Corlu and E. Leclerc, *Biotechnol. Bioeng.*, 2011, **108**, 1704–1715.
25 J. M. Prot, O. Videau, C. Brochot, C. Legallais, H. Benech and E. Leclerc, *Int. J. Pharm.*, 2011, **408**, 67–75.
26 J. M. Prot, A. Bunescu, B. Elena-Hermann, C. Aninat, L. Choucha Snouber, L. Griscom, F. Bois, C. Legallais, C. Brochot, A. Corlu, M. D. Dumas and E. Leclerc, *Toxicol. Appl. Pharmacol.*, 2012, **259**, 270–280.
27 R. Baudoin, G. Alberto, A. Legendre, P. Paullier, M. Naudot, M. J. Fleury, S. Jacques, L. Griscom and E. Leclerc, *Biotechnol. Prog.*, 2014, **30**, 401–410.
28 R. Jellali, T. Bricks, S. Jacques, M. J. Fleury, P. Paullier, M. Merlier and E. Leclerc, *Biopharm. Drug Dispos.*, 2016, **37**, 264–275.
29 R. Baudoin, A. Legendre, S. Jacques, J. Cotton, F. Bois and E. Leclerc, *J. Pharm. Sci.*, 2014, **103**, 706–718.
30 J. B. Houston, *Biochem. Pharmacol.*, 1994, **47**, 1469–1479.
31 J. B. Houston and D. J. Carlile, *Toxicol In Vitro*, 1997, **11**, 473–478.
32 P. O. Seglen, *Exp. Cell Res.*, 1973, **82**, 391–398.
33 R. Baudoin, L. Griscom, J. M. Prot, C. Legallais and E. Leclerc, *Biochem. Eng. J.*, 2011, **53**, 172–181.
34 R. Jellali, P. Paullier, M. J. Fleury and E. Leclerc, *Sens. Actuators, B*, 2016, **229**, 396–407.
35 R. Baudoin, J. M. Prot, G. Nicolas, J. Brocheton, C. Brochot, C. Legallais, H. Benech and E. Leclerc, *Xenobiotica*, 2013, **43**, 140–152.
36 D. Habka, *Modélisation toxico-pharmacocinétique à partir de méthodes bioinformatiques et de tests in vitro*, PhD, Universite de Technologie de Compiegne, France, 2010.
37 K. Ito and J. B. Houston, *Pharm. Res.*, 2004, **21**, 785–792.
38 S. J. Griffin and J. B. Houston, *Drug Metab. Dispos.*, 2005, **33**, 115–120.
39 Y. Naritomi, S. Terashita, A. Kagayama and Y. Sugiyama, *Drug Metab. Dispos.*, 2003, **31**, 580–588.
40 L. E. Witherow and B. Houston, *J. Pharmacol. Exp. Ther.*, 1999, **290**, 58–64.
41 R. Austin, P. Barton, S. Mohmed and R. Riley, *Drug Metab. Dispos.*, 2005, **33**, 419–425.
42 M. Bonati, R. Latini, G. Tognoni, J. F. Young and S. Garattini, *Drug Metab. Rev.*, 1984, **15**, 1355–1383.
43 J. W. Mandema, B. Tuk, A. L. van-Steveninck, D. D. Breimer, A. F. Cohen and M. Danhof, *Clin. Pharmacol. Ther.*, 1992, **51**, 715–728.
44 K. Ménochet, K. E. Kenworthy, J. B. Houston and A. Galetin, *J. Pharmacol. Exp. Ther.*, 2012, **341**, 2–15.
45 P. Kilford, M. Gertz, B. Houston and A. Galetin, *Drug Metab. Dispos.*, 2008, **36**, 1194–1197.
46 U. Zanelli, N. Caradonna, D. Hallifax, E. Turlizzi and B. Houston, *Drug Metab. Dispos.*, 2012, **40**, 104–110.
47 H. S. Brown, A. Chadwick and J. B. Houston, *Drug Metab. Dispos.*, 2007, **35**, 2119–2126.
48 R. J. Riley, D. F. McGinnity and R. P. Austin, *Drug Metab. Dispos.*, 2005, **33**, 1304–1311.
49 P. Lundquist, J. Lööf, U. Fagerholm, I. Sjögren, J. Johansson, S. Briem, J. Hoogstraate, L. Afzelius and T. Andersson, *Drug Metab. Dispos.*, 2014, **42**, 459–468.
50 D. Carlile, Z. Katayoun and B. Houston, *Drug Metab. Dispos.*, 1997, **25**, 903–911.
51 S. Pang and M. Rowland, *J. Pharmacokinet. Biopharm.*, 1977, **5**, 625–653.
52 S. Pang and M. Rowland, *J. Pharmacokinet. Biopharm.*, 1977, **5**, 655–680.
53 M. S. Roberts and M. Rowland, *J. Pharmacokinet. Biopharm.*, 1986, **14**, 227–260.
54 G. Rice, C. Ryan, P. Leiber-Man, R. Mathie, E. McGhee, A. Harper and L. Blumgart, *Br. J. Exp. Pathol.*, 1977, **58**, 236–242.
55 G. M. Pollack, K. L. R. Brouwer, K. B. Demby and J. A. Jones, *Drug Metab. Dispos.*, 1990, **18**, 197–202.
56 H. Jones, H. Barton, Y. Lai, Y. Bi, E. Kimoto, S. Kempshall, S. Tate, A. El-Kattan, B. Houston, A. Galetin and K. Fenner, *Drug Metab. Dispos.*, 2012, **40**, 1007–1017.
57 A. Bortolotti, L. Jiritano and M. Bonati, *Drug Metab. Dispos.*, 1985, **13**, 227–231.
58 Y. Shirasaka, J. Sager, J. Lutz, C. Davis and N. Isoherranen, *Drug Metab. Dispos.*, 2013, **41**, 1414–1424.
59 B. Tuk, M. F. van Oostenbruggen, V. M. M. Herben, J. W. Mandema and M. Danhof, *J. Pharmacol. Exp. Ther.*, 1999, **289**, 1067–1074.
60 H. Jones and K. Rowland-Yeo, *CPT Pharmacometrics. Syst. Pharmacol.*, 2013, **2**, e63.